Mechanics Research Communications 97 (2019) 39–45

Contents lists available at ScienceDirect

Mechanics Research Communications

journal homepage: www.elsevier.com/locate/mechrescom

Stochastic multiscale modeling with random fields of material properties defined on nonconvex domains

S. Chu, J. Guilleminot*

Department of Civil and Environmental Engineering, Duke University, Durham, NC 27708, USA

ARTICLE INFO

Article history:
Received 19 December 2018
Revised 30 January 2019
Accepted 31 January 2019
Available online 1 February 2019

Keywords:
Multiscale analysis
Nonconvex domain
Stochastic methods
Random field
Uncertainty quantification

ABSTRACT

A methodology to model and generate spatially dependent material uncertainties in stochastic multiscale analysis is proposed. The approach consists in defining non-Gaussian random fields through transport maps acting on Gaussian fields, defined by appropriately filtering a Gaussian white noise. In contrast to standard covariance-based representations, the proposed strategy can efficiently accommodate the case of fields with anisotropic correlation structures on nonconvex domains. This case is especially relevant to computational homogenization involving random microstructures with connected phases. The theoretical stochastic framework is first laid down. A numerical application associated with a polydisperse random microstructure is then presented to illustrate various aspects of the method.

1. Introduction

The proper identification, modeling and propagation of uncertainties is of paramount importance in multiscale frameworks [1,2] where stochasticity is typically induced by morphological randomness or material uncertainties, or a combination of both. Accounting for the former type of uncertainties is a classical issue in homogenization theories for random media [3–5]: when the separation of scales can reasonably be invoked, the homogenized property is deterministic, independent of boundary conditions, and it is referred to as an effective property. For non-separated scales, however, the homogenized coefficient presents non-vanishing random fluctuations [6] and is referred to as an apparent property, following the terminology introduced in [7]. The propagation of geometrical uncertainties has been extensively addressed over the past two decades, mostly through Monte Carlo simulations or collocation methods; see [8] for a state-of-the-art review, as well as [9–19] for various examples.

The propagation of material-type uncertainties can be pursued by using similar frameworks (see, e.g., [20–22]) and contributions attempting to combine various forms of parametric uncertainties can be found in [23–27] for some specific classes of materials. In these works, stochastic material parameters are modeled as random variables or more rarely, as random fields. In the latter case, finite-dimensional representations of random fields are usually introduced through truncated Karhunen–Loève expansions [8].

In this paper, we consider spatially varying material properties defined on complex, nonconvex domains. This case has received little attention to date and is relevant to the modeling of, *e.g.*, connected phases in fiber-reinforced composite materials; see Fig. 1 for an illustration.

The nonconvexity exhibited by the domain (occupied by the connected phase) complicates the construction of an appropriate covariance kernel, which in turn restricts the use of covariance-based approaches to define and generate the random field(s) of interest. A possible approach to attack this problem consists in defining an homeomorphic transformation of the domain to address both stochastic modeling and sampling on a much simpler geometry. Such a strategy is, however, hardly applicable in most multiscale setups where the number of topological singularities (heterogeneities) is from moderate to large. In addition, the image of a covariance function through an homeomorphic transformation is generally unknown, so that physical insight may be lost while defining some key properties in the stochastic model. Another way to proceed is to define covariance functions parametrized with a geodesic distance [28]. This approach is a very natural way to use standard (covariance-based) sampling techniques on complex geometries; see [29] for a recent structural application. This strategy is nonetheless restricted, by construction, to isotropic-like covariance structures and may be penalized by its computational cost, especially for three-dimensional microstructures.

An alternative approach enabling the computational treatment of microstructural complexity in the definition and sampling of

* Corresponding author.
E-mail address: johann.guilleminot@duke.edu (J. Guilleminot).

https://doi.org/10.1016/j.mechrescom.2019.01.008
0093-6413/

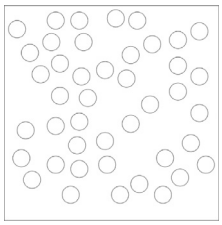

Fig. 1. Example of a random microstructure where the matrix phase constitutes a nonconvex domain in $\mathbb{R}^2$.

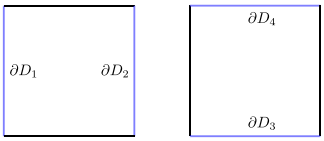

Fig. 2. Boundary indexation for two-dimensional problems.

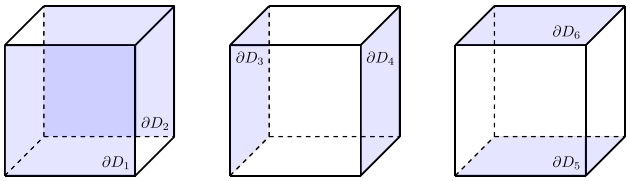

Fig. 3. Boundary indexation for three-dimensional problems.

spatially dependent stochastic material properties is proposed in this paper. The methodology consists in defining the random field of interest through the transformation of an underlying Gaussian field, obtained by filtering the Gaussian white noise with an appropriate diffusion operator. The central idea is to specifically define the components of the matrix-valued diffusion coefficient as velocity fields associated with suitable potential flows, hence naturally capturing the correlation structure around immersed geometries. The rest of this paper is organized as follows. The theoretical framework is first presented in Section 2. The overview of the modeling approach is exposed, and methodological ingredients are next reviewed step by step. An application in computational homogenization of linear microstructures is finally provided in Section 3 to illustrate some salient features of the proposed framework.

2. Mathematical formulation

2.1. Overview of the methodology

Let us consider a random composite made up with n constitutive phases, assumed to exhibit linear or nonlinear elastic behaviors. The statistical volume element under consideration is denoted by $D \subset \mathbb{R}^d$, with $1 \leqslant d \leqslant 3$. Let D be decomposed as $D = \Omega \cup \left(\cup_{i=1}^{n-1} \Omega_i\right)$, with $\Omega_i \cap_{i \neq j} \Omega_j = \emptyset$ and $\Omega \cap \Omega_i = \emptyset$ for $1 \leqslant i, j \leqslant n-1$. The domains $\{\Omega_i\}_{i=1}^{n-1}$ correspond to $(n-1)$ families of heterogeneities, embedded in the matrix phase occupying the connected domain Ω. Let ∂D and $\partial\Omega$ be the boundaries of D and Ω, respectively. For latter use, the boundary ∂D is defined as $\partial D = \cup_{i=1}^{2d} \partial D_i$, where ∂D_j and ∂D_{j+1} denote boundaries located on opposite faces, with $j = 2k-1$ and $1 \leqslant k \leqslant d$; see Figs. 2 and 3.

Let $\{\boldsymbol{P}(\boldsymbol{x}), \boldsymbol{x} \in \Omega\}$ be the second-order random field of material parameters defining the stochastic constitutive model for the matrix phase. This random field is defined on a probability space $(\Theta, \mathcal{F}, \mathcal{P})$ and is assumed to take its values in a subset $\mathcal{S} \subset \mathbb{R}^q$. For linear elastic isotropic solids, the random vector $\boldsymbol{P}(\boldsymbol{x})$ ($\boldsymbol{x}$ being fixed) can be taken as $\boldsymbol{P}(\boldsymbol{x}) = (k(\boldsymbol{x}), \mu(\boldsymbol{x}))$, where $k(\boldsymbol{x})$ and $\mu(\boldsymbol{x})$ are the stochastic bulk and shear moduli at location $\boldsymbol{x}$, and $\mathcal{S} = \mathbb{R}_{>0} \times \mathbb{R}_{>0}$. Given the almost sure boundedness properties typically exhibited by material parameters, the random field $\{\boldsymbol{P}(\boldsymbol{x}), \boldsymbol{x} \in \Omega\}$ is non-Gaussian. Moreover, $\{\boldsymbol{P}(\boldsymbol{x}), \boldsymbol{x} \in \Omega\}$ is assumed to belong to a given subclass of second-order non-Gaussian random fields admitting the representation

$$\boldsymbol{P}(\boldsymbol{x}) = \mathcal{T}(\boldsymbol{\Xi}(\boldsymbol{x}), \boldsymbol{x}), \quad \forall \boldsymbol{x} \in \Omega, \tag{1}$$

where $\mathcal{T}$ is a nonlinear measurable mapping and $\{\boldsymbol{\Xi}(\boldsymbol{x}), \boldsymbol{x} \in \mathbb{R}^d\}$ is a normalized $\mathbb{R}^q$-valued Gaussian random field with independent components. This subclass typically contains mathematically admissible random field models exhibiting both reasonable modeling flexibility and low-dimensional parameterization. The construction of a stochastic model for the field of material properties then involves *(i)* the construction (or identification) of $\mathcal{T}$, and *(ii)* the definition of the Gaussian germ. The latter definition is the central issue addressed in this paper and must ensure that the covariance function for the non-Gaussian random field $\{\boldsymbol{P}(\boldsymbol{x}), \boldsymbol{x} \in \Omega\}$, induced by the mapping $\mathcal{T}$, is geometrically consistent. In this context, the construction of an admissible mapping $\mathcal{T}$ for selected classes of linear and nonlinear behaviors is outside the scope of this paper. Interested readers are referred to [30,31] and [32–35] for the construction of information-theoretic stochastic models in linear and nonlinear elasticity, respectively (see Section 3 for an illustrative example). In particular, the stochastic model proposed in [31] can readily be combined with the presented approach to model elasticity fields with any material symmetry within the class of models defined by Eq. (1) (note for the sake of completeness that spectral expansions for all elasticity fields can be found in [36]).

The approach pursued in this work relies on the interpretation of Gaussian random fields with Matérn-type correlation structures as solutions of stochastic partial differential equations. For stationary fields, the Matérn covariance function $\boldsymbol{\tau} \mapsto C(\boldsymbol{\tau})$ is defined as

$$C(\boldsymbol{\tau}) = \sigma^2 \frac{2^{1-\nu}}{\Gamma(\nu)} (\kappa \|\boldsymbol{\tau}\|)^{\nu} K_{\nu}(\kappa \|\boldsymbol{\tau}\|), \quad \forall \boldsymbol{\tau} \in \mathbb{R}^d, \tag{2}$$

where $\kappa > 0$ and $\nu > 0$ are scale and smoothness parameters, and σ^2 represents the variance of the field. Gaussian fields with the covariance function defined by Eq. (2) are $\lfloor \nu - 1 \rfloor$ mean square differentiable, and the classical exponential and squared exponential covariance functions are obtained for $\nu = 1/2$ and $\nu \to +\infty$, respectively. As noticed by Whittle [37,38] (see, e.g., Section 9 in [37]), a Gaussian field $\{\Xi(\boldsymbol{x}), \boldsymbol{x} \in \mathbb{R}^d\}$ exhibiting the covariance function given by Eq. (2) is the stationary solution of the stochastic partial differential equation (SPDE)

$$\left(\kappa^2 - \langle \boldsymbol{\nabla}, \boldsymbol{\nabla} \rangle\right)^{\alpha/2} \Xi(\boldsymbol{x}) = \dot{\mathcal{W}}(\boldsymbol{x}), \quad \boldsymbol{x} \in \mathbb{R}^d, \tag{3}$$

where $\langle \cdot, \cdot \rangle$ denotes the inner product in $\mathbb{R}^d$, $\boldsymbol{\nabla}$ is the nabla (del) operator, $\alpha = \nu + d/2$ and $\{\dot{\mathcal{W}}(\boldsymbol{x}), \boldsymbol{x} \in \Omega\}$ is the spatial normalized Gaussian white noise. This result was recently revisited along with computational aspects in [39]. In this work, we consider the extension to anisotropic covariance kernels proposed in [40] and define each independent component of $\{\boldsymbol{\Xi}(\boldsymbol{x}), \boldsymbol{x} \in \mathbb{R}^d\}$ as the solution of the SPDE

$$\left(\kappa^2 - \langle \boldsymbol{\nabla}, [H(\boldsymbol{x})] \boldsymbol{\nabla} \rangle\right)^{\alpha/2} \Xi_j(\boldsymbol{x}) = \dot{\mathcal{W}}(\boldsymbol{x}), \quad \boldsymbol{x} \in \Omega, \tag{4}$$

where $\boldsymbol{x} \mapsto [H(\boldsymbol{x})]$ is a diffusion field with values in the set of symmetric positive definite matrices (note that there is no time-dependency and that the term "diffusion" is preserved here for the sake of consistency with [39,40]). The boundary condition associated with Eq. (4) will be specified later on. The definition of this diffusion field and the strategy to solve the SPDE are addressed in order in Sections 2.2 and 2.3.

2.2. Step 1: definition of elementary problems

In order to define the diffusion field in accordance with microstructural complexity, we now introduce a set of d elementary problems, the solutions of which are denoted by $\{\boldsymbol{x}\mapsto\Psi_i(\boldsymbol{x})\}_{i=1}^d$. Assume that $\partial\Omega\cap\partial D_{2i-1}\neq\emptyset$ and $\partial\Omega\cap\partial D_{2i}\neq\emptyset$, $1\leqslant i\leqslant d$. It should be noticed that these geometrical boundary conditions are generally satisfied by random (stationary) microstructures and allow the case of microstructural samples with inclusions intersecting the boundary of D to be handled. Each field $\boldsymbol{x}\mapsto\Psi_i(\boldsymbol{x})$, $1\leqslant i\leqslant d$, is specifically defined as the solution of the following Laplace problem:

$$\triangle\Psi(\boldsymbol{x})=0,\quad\forall\boldsymbol{x}\in\Omega, \tag{5}$$

augmented with the Dirichlet boundary conditions

$$\begin{cases}\Psi(\boldsymbol{x})=0, & \forall\boldsymbol{x}\in\partial\Omega\cap\partial D_{2i-1},\\ \Psi(\boldsymbol{x})=1, & \forall\boldsymbol{x}\in\partial\Omega\cap\partial D_{2i},\end{cases} \tag{6}$$

and with the Neumann boundary condition

$$<\nabla\Psi(\boldsymbol{x}),\boldsymbol{n}(\boldsymbol{x})>=0,\quad\forall\boldsymbol{x}\in\partial\Omega\setminus(\partial D_{2i-1}\cup\partial D_{2i}), \tag{7}$$

where $\boldsymbol{n}(\boldsymbol{x})$ is the outward pointing unit normal vector at point $\boldsymbol{x}$. These solutions are subsequently used to construct vector fields $\{\boldsymbol{x}\mapsto\boldsymbol{e}^i(\boldsymbol{x})\}_{i=1}^d$ corresponding to the normalized velocities of the potential flows described by Eqs. (5)–(7):

$$\boldsymbol{e}^i(\boldsymbol{x})=\frac{1}{\|\nabla\Psi_i(\boldsymbol{x})\|}\nabla\Psi_i(\boldsymbol{x}),\quad\forall\boldsymbol{x}\in\Omega,\quad 1\leqslant i\leqslant d. \tag{8}$$

The fields $\{\boldsymbol{x}\mapsto\boldsymbol{e}^i(\boldsymbol{x})\}_{i=1}^d$ represent physically-consistent correlation paths around the heterogeneities, and can thus be used to appropriately define the diffusion field $\boldsymbol{x}\mapsto[H(\boldsymbol{x})]$ as

$$[H(\boldsymbol{x})]=\sum_{i=1}^d\lambda_i\,\boldsymbol{e}^i(\boldsymbol{x})\otimes\boldsymbol{e}^i(\boldsymbol{x}),\quad\forall\boldsymbol{x}\in\Omega, \tag{9}$$

where $\{\lambda_i>0\}_{i=1}^d$ are model parameters controlling the local anisotropy of the covariance function of $\{\Xi(\boldsymbol{x}),\,\boldsymbol{x}\in\Omega\}$. The form selected in Eq. (9) facilitates the interpretation of the hyperparameters $\{\lambda_i\}_{i=1}^d$ in the local frame defined by the vector fields $\{\boldsymbol{x}\mapsto\boldsymbol{e}^i(\boldsymbol{x})\}_{i=1}^d$. The rationale behind this construction of the diffusion field is that the flows associated with the elementary problems mimic, in some sense, the flow of the matrix phase while the composite material is being processed, and generate natural correlation paths around the heterogeneities.

2.3. Step 2: solving the SPDE

Assume at this stage that $\alpha=2$, and consider a finite element discretization of the domain Ω. In this context, a Galerkin solution of the SPDE is sought in the form

$$\Xi_j(\boldsymbol{x})=\sum_{i=1}^N\eta_i\psi_i(\boldsymbol{x}), \tag{10}$$

where $\{\psi_i\}_{i=1}^N$ is the finite element basis consisting of piecewise linear functions and N is the total number of nodes [39]. Note that the dependence on N of the left-hand side in Eq. (10) is not made explicit for the sake for notational convenience. The weak form is then obtained in a standard manner and can be simplified by applying Green's first identity with Neumann boundary conditions. More specifically, the discretized form involves the $(N\times N)$ matrices $[M]$ and $[G]$ with entries

$$M_{ij}=\int_\Omega\psi_i(\boldsymbol{x})\psi_j(\boldsymbol{x})d\boldsymbol{x} \tag{11}$$

and

$$G_{ij}=\int_\Omega\langle\nabla\psi_i(\boldsymbol{x}),[H(\boldsymbol{x})]\nabla\psi_j(\boldsymbol{x})\rangle d\boldsymbol{x} \tag{12}$$

for $1\leqslant i,\,j\leqslant N$. It can then be shown that the vector of stochastic nodal values satisfies

$$\boldsymbol{\eta}\sim\mathcal{N}(\boldsymbol{0},[\Sigma^{(2)}]), \tag{13}$$

where the covariance matrix $[\Sigma^{(2)}]$ is given by

$$\left[\Sigma^{(2)}\right]=\left(\kappa^2[M]+[G]\right)^{-1}[M]\left(\kappa^2[M]+[G]\right)^{-1} \tag{14}$$

and superscript underpins the order $\alpha=2$. From a computational standpoint, it is more appropriate to work with the precision matrix

$$\left[Q^{(2)}\right]=\left[\Sigma^{(2)}\right]^{-1}=\left(\kappa^2[M]+[G]\right)[M]^{-1}\left(\kappa^2[M]+[G]\right), \tag{15}$$

since $[M]$ and $[G]$ exhibit high sparsity for piecewise linear elements. In addition, the computation of $[Q]$ can be speed up by using the lump mass method to approximate $[M]^{-1}$ as $[M]^{-1}\approx[\widetilde{M}]^{-1}$, where $[\widetilde{M}]$ is the diagonal matrix with elements

$$\widetilde{M}_{ii}=\sum_{j=1}^N M_{ij},\quad 1\leqslant i\leqslant N. \tag{16}$$

A recursion formula on the precision matrix can then be used for arbitrary orders $\alpha\in\mathbb{N}_{>0}$:

$$\left[Q^{(\alpha)}\right]=\left[Q^{(1)}\right][M]^{-1}\left[Q^{(\alpha-2)}\right][M]^{-1}\left[Q^{(1)}\right], \tag{17}$$

with

$$\left[Q^{(1)}\right]=\kappa^2[M]+[G] \tag{18}$$

and $[Q^{(2)}]$ defined by Eq. (15). The use of Eq. (17) enables generating random fields with various mean-square differentiability properties and thus offers significant flexibility in terms of stochastic modeling. It should be noted that the previous derivations can also be extended to non-integer orders

$$\left[Q^{(\alpha)}\right]=[M]^{1/2}\left([M]^{-1/2}[Q^{(1)}][M]^{-1/2}\right)^{\alpha}[M]^{1/2}, \tag{19}$$

for any $\alpha\geqslant 0$, in which case the sparsity of the precision matrix is lost.

Let $[Q^{(\alpha)}]=[L^{(\alpha)}]^{\mathrm{T}}[L^{(\alpha)}]$ be a matrix factorization of $[Q^{(\alpha)}]$, obtained through, *e.g.*, a Cholesky or a QR decomposition. It follows that $\boldsymbol{\eta}$ satisfies the linear system

$$[L^{(\alpha)}]\boldsymbol{\eta}=\boldsymbol{g},\quad\boldsymbol{g}\sim\mathcal{N}(\boldsymbol{0},[I_N]), \tag{20}$$

which can be used to draw samples of the stochastic nodal values (and thus, of the Gaussian random field $\{\Xi_j(\boldsymbol{x}),\,\boldsymbol{x}\in\Omega\}$; see Eq. (10)) from samples of the multidimensional normalized Gaussian probability measure.

It should be noticed that boundary effects are typically introduced while solving the SPDE on bounded domains. This aspect is not an issue in a multiscale framework where the stationarity of the microstructural fields enables the consideration of a sampling domain that is larger than the domain of interest.

2.4. Step 3: definition of non-Gaussian fields of material properties

We now turn to the definition of the non-Gaussian random field $\{\boldsymbol{P}(\boldsymbol{x}),\,\boldsymbol{x}\in\Omega\}$ of material parameters. As previously indicated, we consider non-Gaussian random fields that can be expressed as

$$\boldsymbol{P}(\boldsymbol{x})=\mathcal{T}(\boldsymbol{\Xi}(\boldsymbol{x}),\boldsymbol{x}),\quad\forall\boldsymbol{x}\in\Omega, \tag{21}$$

where $\mathcal{T}$ is a suitable, nonlinear mapping. Information-theoretic random field models for spatially dependent material properties can be found in the references listed below Eq. (1). For the sake of illustration, assume that the elasticity field in the matrix

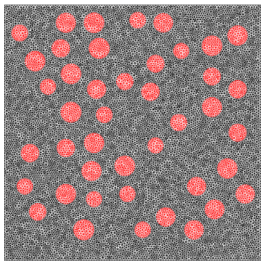

Fig. 4. Finite element mesh of the microstructural sample under consideration.

phase (associated with the nonconvex domain) is isotropic almost surely. In this case, the elasticity random field $\{\mathbb{C}(\boldsymbol{x}), \boldsymbol{x} \in \Omega\}$ can be written as

$$\mathbb{C}(\boldsymbol{x}) = dk(\boldsymbol{x})\mathbb{J} + 2\mu(\boldsymbol{x})\mathbb{K}, \quad \forall \boldsymbol{x} \in \Omega \tag{22}$$

where $\{k(\boldsymbol{x}), \boldsymbol{x} \in \Omega\}$ and $\{\mu(\boldsymbol{x}), \boldsymbol{x} \in \Omega\}$ are the random fields of bulk and shear moduli, and $(\mathbb{J}, \mathbb{K})$ is the standard basis of the set of isotropic tensors in $\mathbb{R}^d$. In this setting, one has $\boldsymbol{P}(\boldsymbol{x}) = (k(\boldsymbol{x}), \mu(\boldsymbol{x}))$, $q = 2$ and one possible choice for the mapping $\mathcal{T}$, consistent with information theory [31,41], is to take

$$k(\boldsymbol{x}) = F^{-1}_{\mathcal{G}(s_1,s_2)}\big(F_{\mathcal{N}(0,1)}(\Xi_1(\boldsymbol{x}))\big), \quad \forall \boldsymbol{x} \in \Omega \tag{23}$$

and

$$\mu(\boldsymbol{x}) = F^{-1}_{\mathcal{G}(s_3,s_4)}\big(F_{\mathcal{N}(0,1)}(\Xi_2(\boldsymbol{x}))\big), \quad \forall \boldsymbol{x} \in \Omega, \tag{24}$$

where $F_{\mathcal{G}(a,b)}$ is the cumulative distribution function of the Gamma law with scale and shape parameters given by a and b, and $F_{\mathcal{N}(0,1)}$ is the cumulative distribution function of the normalized univariate Gaussian law. In this case, the bulk and shear moduli random fields are statistically independent. Alternatively, correlated elastic coefficients can be obtained through the following transformations [42]:

$$k(\boldsymbol{x}) = F^{-1}_{\mathcal{G}(s_1,s_2)}\big(F_{\mathcal{N}(0,1)}(\Xi_1(\boldsymbol{x}))\big) \tag{25}$$

and

$$\mu(\boldsymbol{x}) = F^{-1}_{\mathcal{G}(s_3,s_4)}\Big(F_{\mathcal{N}(0,1)}(\rho\, \Xi_1(\boldsymbol{x}) + \sqrt{1-\rho^2}\, \Xi_2(\boldsymbol{x}))\Big), \tag{26}$$

where ρ denotes the coefficient of correlation between the stochastic bulk and shear moduli.

3. Numerical application

In this section, the proposed framework is used to model the (spatially dependent) stochastic linear elastic properties in the matrix phase of a random microstructure. We consider a polydisperse two-phase microstructure ($n = 2$) in which the positions of the particles are generated by using the molecular-dynamics-based algorithm detailed in [43]. Note that the considered microstructural sample does not exhibit inclusions that intersect the boundary of D. While this characteristics is not critical in the presented application where only material randomness is propagated, it should be emphasized that the proper propagation of both microstructural and material randomness requires domains with intersecting inclusions to be included (this case can easily be handled under the assumptions listed in Section 2.2). The finite element mesh used for subsequent simulations is shown in Fig. 4 and contains 34,372 linear triangular elements.

The properties in the domain Ω_1 occupied by the heterogeneities are taken deterministic and correspond to glass fibers:

$$k_1 = 38.89 \text{ [GPa]}, \quad \mu_1 = 29.17 \text{ [GPa]}. \tag{27}$$

Below, the non-Gaussian model defined by Eqs. (25)–(26) is selected with $\rho = 0.9$, and the hyperparameters (s_1, s_2) and (s_3, s_4) are determined such that $\underline{k} = E\{k(\boldsymbol{x})\} = 3.92$ GPa, $\delta_k = 0.2$, $\underline{\mu} = E\{\mu(\boldsymbol{x})\} = 1.50$ GPa and $\delta_\mu = 0.2$, where E denotes mathematical expectation and δ_X is the coefficient of variation of X. The mean values assigned above correspond to an epoxy matrix.

3.1. Background on computational homogenization

Following the standard approach to computational homogenization for linear elastic microstructures, the homogenized stiffness tensor is defined by using the solution of the following boundary problem:

$$\begin{cases} \operatorname{div}(\boldsymbol{\sigma}) = 0, & \forall \boldsymbol{x} \in D, \\ \boldsymbol{\sigma}(\boldsymbol{x}) = \mathbb{C}^{(D)}(\boldsymbol{x}) : \boldsymbol{\varepsilon}(\boldsymbol{x}), & \forall \boldsymbol{x} \in D, \\ \boldsymbol{\varepsilon}(\boldsymbol{x}) = \nabla^S_{\boldsymbol{x}} \boldsymbol{u}, & \forall \boldsymbol{x} \in D, \end{cases} \tag{28}$$

where $\boldsymbol{\varepsilon}$ and $\boldsymbol{\sigma}$ are the local strain and stress tensors, double dot product between tensors denotes double contraction on nearest indices, $\mathbb{C}^{(D)}$ is the local stiffness tensor in the whole composite domain D, and $\nabla^S_{\boldsymbol{x}}\boldsymbol{u}$ is the symmetrized gradient of the displacement $\boldsymbol{u}$. For the sake of illustration, the above boundary value problem is solved under kinematically uniform boundary conditions:

$$\boldsymbol{u}(\boldsymbol{x}) = \boldsymbol{E}\boldsymbol{x}, \quad \forall \boldsymbol{x} \in \partial D, \tag{29}$$

in which $\boldsymbol{E}$ is a macroscopic strain. Following the works from Huet (see [7], as well as [6]), the response obtained under such boundary conditions provides an upper bound for the overall homogenized tensor and a lower bound can be defined by alternatively considering statically uniform boundary conditions. Note that the study of convergence with respect to the characteristic size of D and boundary conditions, relevant to the issue of scale separation (see [6] and the references therein), is outside the scope of this work and can be achieved through a convergence analysis on appropriate statistical measures [44,45].

The microscopic stiffness random field is decomposed as

$$\mathbb{C}^{(D)}(\boldsymbol{x}) = \mathbb{1}_\Omega(\boldsymbol{x})\mathbb{C}(\boldsymbol{x}) + \mathbb{1}_{\Omega_1}(\boldsymbol{x})\mathbb{C}^{(1)}(\boldsymbol{x}), \quad \forall \boldsymbol{x} \in D, \tag{30}$$

where $\mathbb{1}_S$ is the indicator function of the set S, $\{\mathbb{C}(\boldsymbol{x}), \boldsymbol{x} \in \Omega\}$ is the stiffness tensor random field in the nonconvex matrix phase, and $\boldsymbol{x} \mapsto \mathbb{C}^{(1)}(\boldsymbol{x})$ is the deterministic elasticity field in the inclusion phase, assumed isotropic:

$$\mathbb{C}^{(1)}(\boldsymbol{x}) = 3k_1\mathbb{J} + 2\mu_1\mathbb{K}, \quad \forall \boldsymbol{x} \in \Omega_1, \tag{31}$$

with k_1 and μ_1 given by Eq. (27).

The macroscopic constitutive model then reads as

$$\overline{\boldsymbol{\sigma}} = \widetilde{\mathbb{C}}_{\text{KUBC}} : \boldsymbol{E}, \tag{32}$$

where the overbar denotes the operator of spatial averaging over Ω:

$$\overline{f} = \frac{1}{|\Omega|}\int_\Omega f(\boldsymbol{x})\, d\boldsymbol{x}, \tag{33}$$

and $|\Omega|$ is the measure element of Ω. The stochastic overall stiffness tensor is given by:

$$\widetilde{\mathbb{C}}_{\text{KUBC}} = \overline{\mathbb{C}^{(D)} : \mathbb{A}}, \tag{34}$$

where $\mathbb{A}$ is the so-called strain localization tensor such that

$$\mathbb{A}_{ijk\ell} = \boldsymbol{\varepsilon}_{ij}(\boldsymbol{E}^{(k\ell)}), \tag{35}$$

and $\boldsymbol{\varepsilon}(\boldsymbol{E}^{(k\ell)})$ is the strain field solution to the boundary value problem in Eq. (28), substituting $\boldsymbol{E}^{(k\ell)}$ for $\boldsymbol{E}$ in Eq. (29), with the set $\{\boldsymbol{E}^{(k\ell)}\}_{k,\ell}$ of rank-2 tensors defined as

$$\boldsymbol{E}^{(k\ell)}_{ij} = \frac{1}{2}\big(\delta_{ik}\delta_{j\ell} + \delta_{i\ell}\delta_{jk}\big). \tag{36}$$

In practice, the propagation of material uncertainties across the scales can be performed by using any stochastic solver. The choice

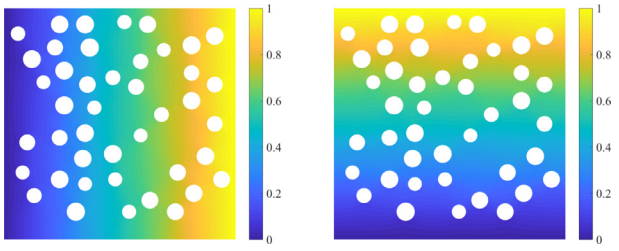

Fig. 5. Plot of the vector fields $\boldsymbol{x} \mapsto \Psi_1(\boldsymbol{x})$ (left) and $\boldsymbol{x} \mapsto \Psi_2(\boldsymbol{x})$ (right).

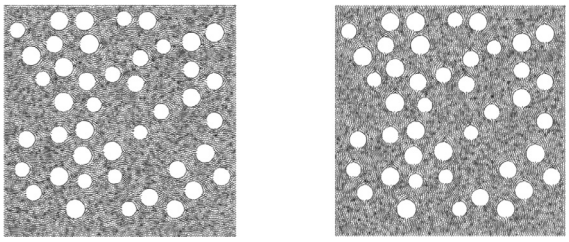

Fig. 6. Plot of the vector fields $\boldsymbol{x} \mapsto \boldsymbol{e}^1(\boldsymbol{x})$ (left) and $\boldsymbol{x} \mapsto \boldsymbol{e}^2(\boldsymbol{x})$ (right).

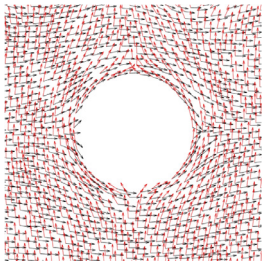

Fig. 7. Plot of the vector fields $\boldsymbol{x} \mapsto \boldsymbol{e}^1(\boldsymbol{x})$ (black lines) and $\boldsymbol{x} \mapsto \boldsymbol{e}^2(\boldsymbol{x})$ (red lines) around an inclusion (seen as a hole). (For interpretation of the references to color in this figure legend, the reader is referred to the web version of this article.)

of an appropriate solver is generally problem specific and is not the purpose of the present work: interested readers are referred to the series of reviews provided in [8] for relevant discussions.

3.2. Application to a polydisperse random microstructure

The first step in the methodology consists in constructing the vector fields defining the correlation paths within the domain Ω (the inclusions are hence viewed as holes while defining and sampling the random field); see Section 2.2. In the sequel, the two boundary value problems defined by Eqs. (5)–(7) (for $i \in \{1, 2\}$) are solved by a standard finite element formulation with 28,496 linear triangular elements. The solution fields $\{\boldsymbol{x} \mapsto \Psi_i(\boldsymbol{x})\}_{i=1}^2$ are shown in Fig. 5.

The local basis vectors associated with the fields $\{\boldsymbol{x} \mapsto \Psi_i(\boldsymbol{x})\}_{i=1}^2$ over the entire microstructural sample are shown in Fig. 6, while the vector fields around a given inclusion (recall that the latter is seen as a hole at this stage) can be seen in Fig. 7. Within the proposed approach, these vector fields are used to define the diffusion field through Eq. (9).

Next, the Gaussian random fields $\{\{\Xi_i(\boldsymbol{x}), \boldsymbol{x} \in \Omega\}\}_{i=1}^2$ are sampled by using the SPDE approach reviewed in Section 2.3, for $\alpha = 2$, $\kappa = 50$ and various choices of $\boldsymbol{\lambda} = (\lambda_1, \lambda_2)$. In order to illustrate the flexibility of the framework, an isotropic correlation kernel is considered, with $\boldsymbol{\lambda} = (10, 10)$, and anisotropic correlation kernels are also selected with $\boldsymbol{\lambda} = (100, 10)$ and $\boldsymbol{\lambda} = (500, 10)$. These choices allows us to model and explore the impact of a larger correlation range along the direction defined by the vector field $\boldsymbol{x} \mapsto \boldsymbol{e}^1(\boldsymbol{x})$, oriented from ∂D_1 to ∂D_2 (see Fig. 2).

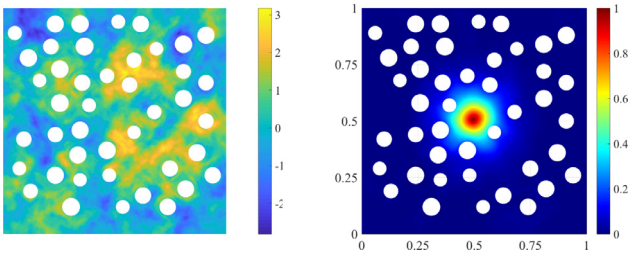

Fig. 8. Plot of one realization of the Gaussian field (left) and estimated correlation function (right) for a quasi-isotropic kernel: $\boldsymbol{\lambda} = (10, 10)$.

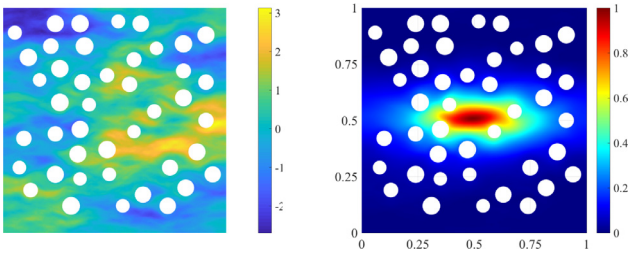

Fig. 9. Plot of one realization of the Gaussian field (left) and estimated correlation function (right) for a moderately anisotropic kernel: $\boldsymbol{\lambda} = (100, 10)$.

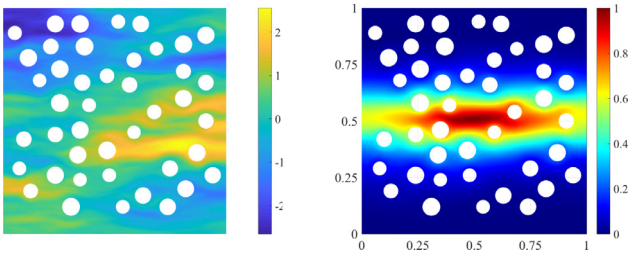

Fig. 10. Plot of one realization of the Gaussian field (left) and estimated correlation function (right) for a strongly anisotropic kernel: $\boldsymbol{\lambda} = (500, 10)$.

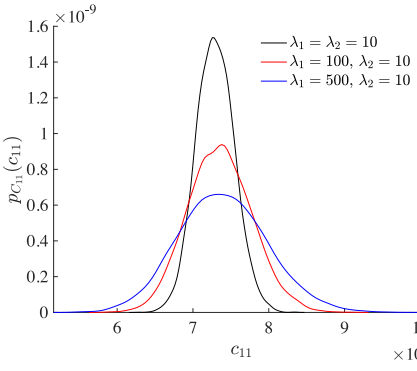

Fig. 11. Estimated probability functions of the homogenized coefficient C_{11}, obtained for different covariance kernels.

The qualitative impact of such choices can be seen in Figs. 8–10, where realizations and correlation functions (estimated with 20,000 independent samples) of the Gaussian field are shown for the three retained configurations. Note that the samples are obtained by using the same realization of the Gaussian random vector $\boldsymbol{g}$ in Eq. (20), for the sake of comparison, and that the point $\boldsymbol{x}^{(0)} = (0.5, 0.5)$ serves as the reference point for estimating the correlation.

The impact of the parametrization in the diffusion field is clearly observed, and it is seen that the correlation function with the most pronounced anisotropy incorporates the presence of the heterogeneities. Finally, the uncertainty propagation was

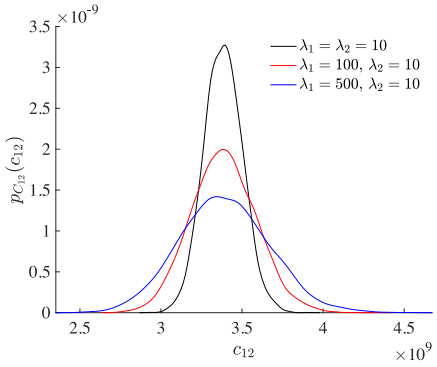

Fig. 12. Estimated probability functions of the homogenized coefficient C_{12}, obtained for different covariance kernels.

performed using a Monte Carlo approach with 10,000 independent realizations of the random fields. The probability density functions of the homogenized coefficients C_{11} and C_{12} (in Voigt notation) are shown in Figs. 11 and 12, respectively.

4. Conclusion

A novel methodology to model and generate spatially dependent material uncertainties in stochastic multiscale analysis was proposed. More specifically, the approach consists in defining non-Gaussian random fields through transformations of a filtered Gaussian white noise. In contrast to standard covariance-based representations, the proposed strategy can efficiently accommodate the case of anisotropic correlation structures on nonconvex domains. A multiscale application involving a prototypical random microstructure was presented to illustrate various aspects of the method. While the probabilistic framework has been demonstrated on elasticity fields, it can readily be applied to model other spatially varying stochastic properties, such as nonlinear mechanical properties and conductivity.

Acknowledgments

The second author (JG) acknowledges the support from the National Science Foundation under Grant no. CMMI-1726403.

References

[1] A. Chernatynskiy, S.R. Phillpot, R. LeSar, Uncertainty quantification in multiscale simulation of materials: a prospective, Ann. Rev. Mater. Res. 43 (1) (2013) 157–182, doi:10.1146/annurev-matsci-071312-121708.
[2] K. Matouš, M.G.D. Geers, V.G. Kouznetsova, A. Gillman, A review of predictive nonlinear theories for multiscale modeling of heterogeneous materials, J. Comput. Phys. 330 (2017) 192–220, doi:10.1016/j.jcp.2016.10.070.
[3] T. Mura, Micromechanics of Defects in Solids, Springer, the Netherlands, 1987.
[4] S. Nemat-Nasser, M. Hori, Micromechanics: Overall Properties of Heterogeneous Materials, North-Holland, 1993.
[5] S. Torquato, Random Heterogeneous Materials: Microstructure and Macroscopic Properties, Springer, New York, 2002.
[6] M. Ostoja-Starzewski, Microstructural Randomness and Scaling in Mechanics of Materials, Chapman and Hall/CRC, 2008.
[7] C. Huet, Application of variational concepts to size effects in elastic heterogeneous bodies, J. Mech. Phys. Solids 38 (6) (1990) 813–841, doi:10.1016/0022-5096(90)90041-2.
[8] R. Ghanem, D. Higdon, H. Owhadi, Handbook of Uncertainty Quantification, Springer, Cham, 2017.
[9] M. Ostoja-Starzewski, Random field models of heterogeneous materials, Int. J. Solids Struct. 35 (19) (1998) 2429–2455, doi:10.1016/S0020-7683(97)00144-3.
[10] S.C. Baxter, L.L. Graham, Characterization of random composites using moving-window technique, J. Eng. Mech. 126 (4) (2000) 389–397, doi:10.1061/(ASCE)0733-9399(2000)126:4(389).
[11] L. Graham, S. Baxter, Simulation of local material properties based on moving-window GMC, Probab. Eng. Mech. 16 (4) (2001) 295–305, doi:10.1016/S0266-8920(01)00022-4.
[12] L. Graham, K. Gurley, F. Masters, Non-gaussian simulation of local material properties based on a moving-window technique, Probab. Eng. Mech. 18 (3) (2003) 223–234, doi:10.1016/S0266-8920(03)00026-2.
[13] M.S. Greene, Y. Liu, W. Chen, W.K. Liu, Computational uncertainty analysis in multiresolution materials via stochastic constitutive theory, Comput. Methods Appl. Mech. Eng. 200 (1) (2011) 309–325, doi:10.1016/j.cma.2010.08.013.
[14] B. Hiriyur, H. Waisman, G. Deodatis, Uncertainty quantification in homogenization of heterogeneous microstructures modeled by xfem, Int. J. Numer. Methods Eng. 88 (3) (2011) 257–278, doi:10.1002/nme.3174.
[15] A. Clément, C. Soize, J. Yvonnet, Computational nonlinear stochastic homogenization using a non-concurrent multiscale approach for hyperelastic heterogeneous microstructures analysis, Int. J. Numer. Methods Eng. 91 (8) (2012) 799–824, doi:10.1002/nme.4293.
[16] A. Clément, C. Soize, J. Yvonnet, Uncertainty quantification in computational stochastic multiscale analysis of nonlinear elastic materials, Comput. Methods Appl. Mech. Eng. 254 (2013) 61–82, doi:10.1016/j.cma.2012.10.016.
[17] S. Dimitris, G. Stefanou, M. Papadrakakis, G. Deodatis, Homogenization of random heterogeneous media with inclusions of arbitrary shape modeled by XFEM, Comput. Mech. 54 (5) (2014) 1221–1235, doi:10.1007/s00466-014-1053-x.
[18] G. Stefanou, D. Savvas, M. Papadrakakis, Stochastic finite element analysis of composite structures based on mesoscale random fields of material properties, Comput. Methods Appl. Mech. Eng. 326 (2017) 319–337, doi:10.1016/j.cma.2017.08.002.
[19] K.A. Acton, S.C. Baxter, Characterization of random composite properties based on statistical volume element partitioning, J. Eng. Mech. 144 (2) (2018) 04017168, doi:10.1061/(ASCE)EM.1943-7889.0001396.
[20] M. Tootkaboni, L. Graham-Brady, A multi-scale spectral stochastic method for homogenization of multi-phase periodic composites with random material properties, Int. J. Numer. Methods Eng. 83 (1) (2010) 59–90, doi:10.1002/nme.2829.
[21] M. Kaminski, The Stochastic Perturbation Method for Computational Mechanics, Wiley, 2013.
[22] L. Mehrez, J. Fish, V. Aitharaju, W.R. Rodgers, R. Ghanem, A PCE-based multiscale framework for the characterization of uncertainties in complex systems, Comput. Mech. 61 (1) (2018) 219–236, doi:10.1007/s00466-017-1502-4.
[23] S. Rahman, A. Chakraborty, A stochastic micromechanical model for elastic properties of functionally graded materials, Mech. Mater. 39 (6) (2007) 548–563, doi:10.1016/j.mechmat.2006.08.006.
[24] R. Bostanabad, B. Liang, J. Gao, W.K. Liu, J. Cao, D. Zeng, X. Su, H. Xu, Y. Li, W. Chen, Uncertainty quantification in multiscale simulation of woven fiber composites, Comput. Methods Appl. Mech. Eng. 338 (2018) 506–532, doi:10.1016/j.cma.2018.04.024.
[25] X.-Y. Zhou, P. Gosling, Influence of stochastic variations in manufacturing defects on the mechanical performance of textile composites, Compos. Struct. 194 (2018) 226–239, doi:10.1016/j.compstruct.2018.04.003.
[26] F.-Y. Zhu, S. Jeong, H.J. Lim, G.J. Yun, Probabilistic multiscale modeling of 3d randomly oriented and aligned wavy CNT nanocomposites and RVE size determination, Compos. Struct. 195 (2018) 265–275, doi:10.1016/j.compstruct.2018.04.060.
[27] S. Jeong, F. Zhu, H. Lim, Y. Kim, G.J. Yun, 3d stochastic computational homogenization model for carbon fiber reinforced CNT/EPOXY composites with spatially random properties, Compos. Struct. 207 (2019) 858–870, doi:10.1016/j.compstruct.2018.09.025.
[28] J.S.B. Mitchell, D.M. Mount, C.H. Papadimitriou, The discrete geodesic problem, SIAM J. Comput. 26 (4) (1987) 647–668, doi:10.1137/0216045.
[29] C. Scarth, S. Adhikari, P.H. Cabral, G.H. Silva, A.P. do Prado, Random field simulation over curved surfaces: applications to computational structural mechanics, Comput. Methods Appl. Mech. Eng. 345 (2019) 283–301, doi:10.1016/j.cma.2018.10.026.
[30] C. Soize, Non-gaussian positive-definite matrix-valued random fields for elliptic stochastic partial differential operators, Comput. Methods Appl. Mech. Eng. 195 (1) (2006) 26–64, doi:10.1016/j.cma.2004.12.014.
[31] B. Staber, J. Guilleminot, Stochastic modeling and generation of random fields of elasticity tensors: a unified information-theoretic approach, Comptes Rendus Mécanique 345 (6) (2017) 399–416, doi:10.1016/j.crme.2017.05.001.
[32] B. Staber, J. Guilleminot, Stochastic modeling of a class of stored energy functions for incompressible hyperelastic materials with uncertainties, Compte rendus Mécanique 349 (2015) 503–514, doi:10.1016/j.crme.2015.07.008.
[33] B. Staber, J. Guilleminot, Stochastic modeling of the Ogden class of stored energy functions for hyperelastic materials: the compressible case, ZAMM J. Appl. Math. Mech. 97 (2017) 273–295, doi:10.1002/zamm.201500255.
[34] L.A. Mihai, T.E. Woolley, A. Goriely, Stochastic isotropic hyperelastic materials: constitutive calibration and model selection, Proc. R. Soc. Lond. A: Math. Phys. Eng. Sci. 474 (2211) (2018), doi:10.1098/rspa.2017.0858.
[35] B. Staber, J. Guilleminot, C. Soize, J. Michopoulos, A. Iliopoulos, Stochastic modeling and identification of a hyperelastic constitutive model for laminated composites, Comput. Methods Appl. Mech. Eng. 347 (2019) 425–444, doi:10.1016/j.cma.2018.12.036.
[36] A. Malyarenko, M. Ostoja-Starzewski, A random field formulation of Hooke's law in all elasticity classes, J. Elast. 127 (2) (2017) 269–302, doi:10.1007/s10659-016-9613-2.
[37] P. Whittle, On stationary processes in the plane, Biometrika 41 (3–4) (1954) 434–449, doi:10.1093/biomet/41.3-4.434.
[38] P. Whittle, Stochastic processes in several dimensions, Bull. Int. Stat. Inst. 40 (1963) 974–994.
[39] F. Lindgren, H. Rue, J. Lindström, An explicit link between Gaussian fields and Gaussian Markov random fields: the stochastic partial differential

equation approach, J. R. Stat. Soc.: Ser. B (Stat. Methodol.) 73 (4) (2011) 423–498, doi:10.1111/j.1467-9868.2011.00777.x.

[40] G.-A. Fuglstad, F. Lindgren, D. Simpson, H. Rue, Exploring a new class of non-stationary spatial Gaussian random fields with varying local anisotropy, Stat. Sin. 25 (1) (2015) 115–133, doi:10.5705/ss.2013.106w.

[41] J. Guilleminot, C. Soize, On the statistical dependence for the components of random elasticity tensors exhibiting material symmetry properties, J. Elast. 111 (2) (2013) 109–130, doi:10.1007/s10659-012-9396-z.

[42] D.-A. Hun, J. Guilleminot, J. Yvonnet, M. Bornert, Stochastic multi-scale modeling of crack propagation in random heterogeneous media, Submitted for publication, (2019).

[43] M. Skoge, A. Donev, F.H. Stillinger, S. Torquato, Packing hyperspheres in high-dimensional Euclidean spaces, Phys. Rev. E 74 (2006) 041127, doi:10.1103/PhysRevE.74.041127.

[44] T. Kanit, S. Forest, I. Galliet, V. Mounoury, D. Jeulin, Determination of the size of the representative volume element for random composites: statistical and numerical approach, Int. J. Solids Struct. 40 (13) (2003) 3647–3679, doi:10.1016/S0020-7683(03)00143-4.

[45] C. Soize, Tensor-valued random fields for meso-scale stochastic model of anisotropic elastic microstructure and probabilistic analysis of representative volume element size, Probab. Eng. Mech. 23 (2) (2008) 307–323, doi:10.1016/j.probengmech.2007.12.019.